Relaxation of surface profiles by evaporation dynamics

Johannes Hager
Fachbereich Physik, Universität Essen, D-45117 Essen, Germany
(Received 11 February 1997; revised manuscript received 29 April 1997)

We present simulations of the relaxation towards equilibrium of one-dimensional steps and sinusoidal grooves imprinted on a surface below its roughening transition. We use a generalization of the hypercube stacking model of Forrest and Tang that allows for temperature-dependent next-nearest-neighbor interactions. For the step geometry the results at $T=0$ agree well with the $t^{1/4}$ prediction of continuum theory for the spreading of the step. In the case of periodic profiles we modify the mobility for the tips of the profile and find the approximate solution of the resulting free boundary problem to be in reasonable agreement with the $T=0$ simulations. [S0163-1829(97)01539-7]

I. INTRODUCTION

The relaxation of corrugated crystal surfaces above their roughening transition is well understood in terms of continuum theory.[1] Experiments[2] and Monte Carlo simulations[3,4] on the decay of sinusoidal grooves agree quantitatively with the predictions of continuum theory and even deviations due to the anisotropy of the surface free energy have been observed.[5] For profiles imprinted on a crystal facet below its roughening transition things are less settled. Several predictions of continuum theories[6–10] for time and wavelength dependence of the decay exist, where differences are mainly due to the different treatment of the singularity in the surface free energy that emerges for the orientation below the roughening temperature T_R. Experiments[2] where surface diffusion prevails show trapezoidal profiles with flat tops and bottoms, a feature qualitatively reproduced by several continuum approaches.[8,10] Simulations below T_R are severely hampered by the slow decay kinetics, a problem somewhat less important for evaporation dynamics. Furthermore, for $T<T_R$ lattice effects play a role that is not present for $T>T_R$ and that is not taken into account in the continuum theory. To suppress these effects, larger systems need to be simulated. The scope of this paper is to present Monte Carlo simulations for the case of evaporation dynamics, which are able to test the predictions of continuum theory. In Sec. II we introduce a modified version of the hypercube stacking model[11] for the case of a two-dimensional surface. In Sec. III we recall the results of continuum theory for a bunch of straight steps and compare them to simulations at $T=0$. In Sec. IV we show how one can modify the continuum theory for periodic grooves to get agreement with our $T=0$ simulations and discuss another recent attempt at this problem. In Sec. V we give a conclusion of our findings. The Appendix briefly describes the core part of our modifications of the hypercube stacking model.

II. MODIFIED HYPERCUBE STACKING MODEL

We use the hypercube stacking model of Forrest and Tang, which is a solid on solid (SOS) model of the (111) surface of a simple cubic crystal as described in Ref. 11. Originally Blöte and Hilhorst[12] considered an antiferromagnetic Ising model on a triangular lattice with anisotropic couplings $K_1=\beta E=K$, $K_2=K+\beta E_2$, and $K_3=K+\beta E_3$ in the limit $K\to-\infty$. They noted already that in two dimensions each Ising-spin configuration can be mapped on a SOS height configuration. In the isotropic case $K_1=K_2=K_3$ considered in Ref. 11 each configuration is a ground state of an antiferromagnetic Ising model with one frustrated bond per triangle and the corresponding SOS model can be considered as temperature independent ($E_2=E_3=0$) or as being at infinite temperature ($\beta\to0$ but $K\to-\infty$). All possible surface configurations have the same energy, since the number of broken nearest neighbor bonds is conserved. Dynamics can be imposed by assigning the same rate p_0 to all evaporation and condensation events allowed by the SOS restriction. Spin flips that maintain the condition of having one frustrated bond per triangle correspond to adding or removing an atom without violating the SOS condition.

We now introduce next-nearest-neighbor interactions of strength J. If an atom is removed from the surface the surface energy changes by $\Delta E=(J/2)\,\Delta n=J(n-3)$, where Δn is the difference in the number of broken next-nearest-neighbor bonds and $n\in\{0,...,6\}$ is the number of next-nearest neighbors in the same layer. Thus the total surface energy is proportional to the number of broken next-nearest-neighbor bonds. We impose the usual Metropolis rates

$$w=\begin{cases} p_0 q^{n-3} & \text{if } n>3 \\ p_0 & \text{if } n\leqslant 3 \end{cases} \tag{1}$$

with $q=\exp[-(J/k_BT)]$ for an evaporation event and

$$w=\begin{cases} p_0 q^{3-n} & \text{if } n<3 \\ p_0 & \text{if } n\geqslant 3 \end{cases} \tag{2}$$

for a condensation event. Note that these rates fulfill detailed balance.

As shown in detail in Ref. 11 the spin representation of the model can be programmed very efficiently by using a multisite coding algorithm, where each spin is coded by a single bit of an integer variable and the dynamics is incorporated via logical operations on the integers. In this type of algorithm we can also incorporate the next-nearest-neighbor interactions between surface atoms as will be shown in some detail in the Appendix. We use four dynamical sublattices as

in Ref. 13 for the evolution of the height profile. The active sublattice is chosen at random and each evaporation or condensation event on that sublattice allowed by the SOS restriction takes place with the Metropolis rate p of the event determined by Eqs. (1) and (2) with $p_0 = 1/2$. Our generalization of the model of Ref. 11 leads to a fast and memory saving implementation of a solid on solid model, which we use in following to study the decay of surface corrugations consisting of many steps. We should note that, due to the multisite coding, where we use each bit of a random number to update one spin, the values of q, and therefore the available temperatures, are restricted to $q \in \{0, k/2^m, 1\}$ with m integer and k odd integer between 1 and $(2^m - 1)$.[11] The best performance of the algorithm is achieved for small m since $3m+1$ random integers are needed for each update of the spins stored in one integer. The cases $q \in \{0,1\}$ (corresponding to $T=0$ and $T=\infty$) need only one random number per update for the rate $p_0 = 1/2$ while $q = 1/2$ (corresponding to $T = 1.44 J/k_B$) needs already four, namely one for $p_0 = 1/2$ and three for $q^3 = 1/8$. After completion of this work we became aware of Ref. 23, where the same kind of model (interpreted as a fcc crystal) with different rates is studied for periodic grooves at a temperature $T = 0.68 T_R$ (corresponding to $q = 1/2$).

In the following we concentrate on the case $T=0$. Then evaporation or condensation events can take place only at (11) steps since adding or removing an atom there does not increase the number of broken bonds. Decay kinetics is slowed down considerably by this choice, but as an advantage nucleation of islands or holes on terraces is entirely absent. This simplifies the comparison to continuum theory, since now the mobility of the surface is proportional to the kink density. The (11) steps are rough even at $T=0$ due to the random update of growth and evaporation sites and the interaction between steps in this limit is purely entropic. We study the relaxation of two different initial profiles, a train of equidistant (11) steps separating two plane (111) surfaces (step geometry) and a periodic sinusoidal corrugation of wavelength L. For the second we grow an initial profile that satisfies $h(x,0) \leqslant \{\mathrm{aint}[\sin(L/2\pi)\, x]\}$ (where aint denotes the integer part of the argument) on a flat surface of size $L \times L$ so that the steps of the profile do have (11) orientation. For the original model, which is effectively at $T=\infty$, we recover the well-known results of Mullins[1] valid above the roughening transition.

III. STEP GEOMETRY

A. Continuum theory

To describe the flattening of a profile under evaporation dynamics with a continuum theory we use the usual assumption that the profile evolution minimizes the free energy of the surface in the most direct way:

$$\frac{\partial}{\partial t} h = -\mu(u) \frac{\delta F}{\delta h}. \tag{3}$$

Here $\mu(u)$ is the mobility of a surface of slope $u = \partial h/\partial x$ and the free energy F of the surface is given by the integral over the free energy $\sigma(u)$ per unit projected surface area. Below the roughening transition $\sigma(u)$ is written as[14]

$$\sigma(u) = \sigma_0 + \sigma_1 |u| + \frac{1}{\gamma} \sigma_\gamma |u|^\gamma + \cdots, \tag{4}$$

with $\gamma = 3$ for purely entropic step repulsion. σ_0 describes the energy of the (111) surface, σ_1 is the step free energy that contributes proportional to the step density $|u|$, and the σ_γ term describes step-step interactions. Now the wedge singularity of the σ_1 term at $u=0$ leads to a δ-function singularity in Eq. (3). In the case of evaporation dynamics well below T_R, where thermally activated nucleation is negligible and the whole dynamics is due to step motion, the mobility of a surface is proportional to the step density[7]

$$\mu(u) = \mu_1 |u|. \tag{5}$$

Since nucleation is an activated process, it is entirely absent in our $T=0$ simulations and Eq. (5) is valid even for a driven surface. Now the vanishing mobility at $u=0$ for the high-symmetry orientation cancels the δ-function singularity in Eq. (3) leading to[7,8]

$$\frac{\partial}{\partial t} h = \mu_1 \sigma_\gamma (\gamma - 1) |u|^{\gamma - 1} \frac{\partial^2}{\partial x^2} h. \tag{6}$$

For the step geometry[8] the scaling ansatz $h(x,t) = \Phi(t^{-\alpha} x)$ gives $\alpha = 1/(\gamma+1)$ and leads to a Barenblatt solution[15,16] for the slope

$$u(x,t) = c_0 t^{-\alpha} (a^2 - y^2)_+^{1/(\gamma-1)}, \tag{7}$$

where $y = x/t^\alpha$, c_0 and a are constants determined by the initial condition and $+$ denotes the positive part of the bracket. Since Eq. (6) is invariant under the rescaling $\bar{x} = x/L, \bar{h} = h/L$ and $\bar{t} = t/L^2$, the whole L dependence for a set of initial profiles of the same slope u but of different size L can be absorbed by rescaling. This leads to $c_0 \sim L^0$ and $a^2 \sim L^{2-4\alpha}$ for the coefficients of Eq. (7).

B. Simulational results

How do these results compare with our $T=0$ simulations? Figure 1 displays the evolution of a step train of 11 steps on a 360×360 lattice up to $t = 10^4$ Monte Carlo steps with $\Delta t = 500$. The height is averaged over the columns parallel to the average step direction and over 10^3 independent runs. To check Eq. (7) and the L dependence of the parameter c_0 and a we plot the scaled slope $u t^{1/4}$ against the scaled width $x t^{-1/4}$ using $\gamma = 3$. Figure 2 displays the flattening data for three step trains of 45, 22, and 11 steps with the same initial slope. The topmost curves are data for 45 steps on a 1440×1440 lattice up to $t = 10^4$ with $\Delta t = 10^3$, averaged over 100 independent runs. The middle set gives the same information for 22 steps on a 720×720 lattice with $\Delta t = 500$ averaged over 10^3 runs and the lowest set are the differentiated data of Fig. 1. The curves of Fig. 2 nicely approach the ellipses of the Barenblatt solution (7) and a good fit can be achieved with $c_0 = 0.028$ and $a^2 = 1024$, 500.4, 250.3 (from top to bottom) in agreement with $c_0 \sim L^0$ and $a^2 \sim L$. The slight skewness in the initial condition (due to computational convenience) vanishes in time, indicating that the Barenblatt

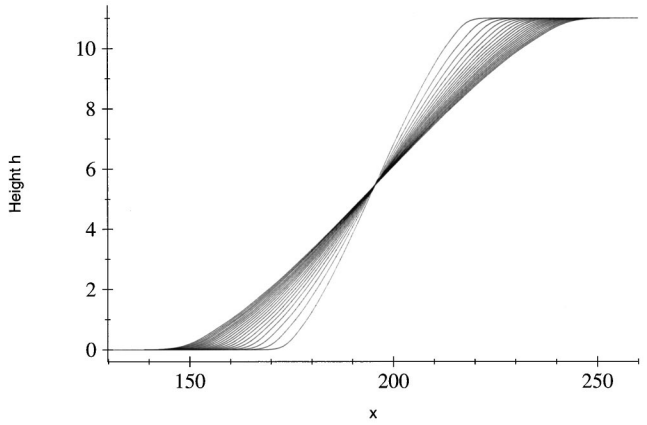

FIG. 1. Flattening of a step train of 11 initially equidistant steps on a 360×360 lattice up to $t=10^4$ Monte Carlo steps with $\Delta t=500$.

solution is attractive also for asymmetric initial profiles. The singularity of Eq. (7) for $u=0$ is smeared out by the fluctuations of the rightmost and leftmost steps. Furthermore, one can resolve the mean positions of the individual steps, as is seen best for the 11-step data. Similar features have been observed recently[17] for two steps with surface diffusion dynamics.

IV. PERIODIC GROOVES

A. Continuum theory

For periodic surface grooves Eq. (6) leads to a solution that predicts a nonparabolic sharpening of the profile tips proportional to $(\delta x)^{(\gamma+1)/\gamma}$ (Refs. 7 and 8) that was observed neither in previous[4,17–19] nor in the present simulations. As pointed out by Rettori and Villain[6] the decay of the profile tips proceeds via the shrinking of islands formed by the two topmost meandering steps, which annihilate each other on contact. This process induces a nonzero mean kink density at the tips of the profile and hence the mobility does not vanish for $u=0$. In this case we expect the wedge singularity of Eq. (5) to be rounded to an analytical function with nonzero

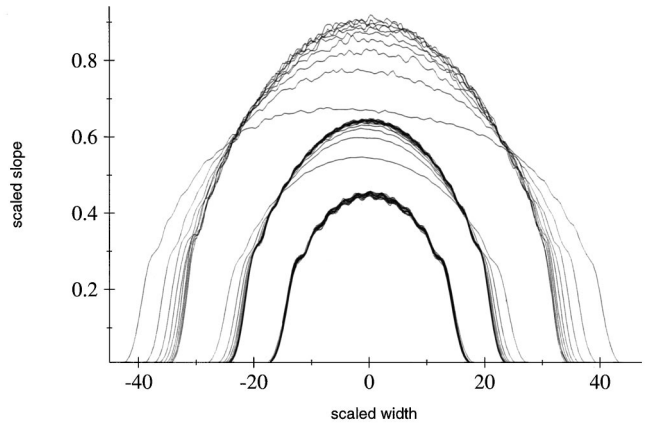

FIG. 2. Time evolution of the scaled slope $ut^{1/4}$ plotted versus the scaled width $xt^{-1/4}$ for step trains of 45, 22, and 11 steps (from top to bottom) with the same initial slope.

$\mu(0)=\mu_0$. Differentiating Eq. (3) with respect to x and performing the functional derivate we get

$$\frac{\partial}{\partial t}u=\frac{\partial}{\partial x}\left(\mu(u)\,\frac{\partial}{\partial x}\sigma'(u)\right)=\mu'(u)\frac{\partial v}{\partial u}\left(\frac{\partial u}{\partial x}\right)^2+\mu(u)\frac{\partial^2 v}{\partial u^2}\left(\frac{\partial u}{\partial x}\right)^2+\mu(u)\frac{\partial v}{\partial u}\frac{\partial^2 u}{\partial x^2},\tag{8}$$

where $v=\sigma'(u)$. Provided that $\mu(u)$ contains no L dependence Eq. (8) is independent under the rescaling $\bar{x}=x/L, h=h/L$ and $\bar{t}=t/L^2$. Thus the data for a set of initial profiles with the same slope but different wavelengths L should collapse on a single scaling curve under the rescaling. Note that the first two terms in Eq. (8) are positive while the third one is negative. In the following we restrict the discussion to the interval $x\in[0,L/4]$, where $u\geqslant0$, which is sufficient to describe the whole profile by symmetry and periodicity. After initial transients have died out we expect $\partial_t u<0$ for all $u>0$, so the third term is dominant in Eq. (8) for $u>0$. For $u\to0$ and $\gamma>2$ the first term in Eq. (8) is much smaller than the second since $\mu'(u)\to0$. In the step flow regime, where Eq. (5) is valid and the third term dominates, the first term is of the same magnitude as the second. By neglecting the first term in Eq. (8) we get

$$\frac{\partial}{\partial t}u=\mu(u)\frac{\partial^2 v}{\partial x^2}.\tag{9}$$

Now the singularity in the free energy is not canceled by a vanishing mobility and gives rise to a δ' function in $\partial^2 v/\partial x^2$. Bonzel and Preuss[10] smoothened the wedge singularity and solved the resulting equation numerically in the case of surface diffusion. This leads to qualitatively correct results but introduces additional parameters. As required by the thermodynamic stability of neighboring surface orientations with $u\neq0$, $v=\sigma'(u)$ is strictly increasing and therefore invertible. So we can transform the singular equation (9) into a well-defined free boundary problem[8] by using v instead of u as the independent variable. Note that for a singular orientation with unstable neighbor orientations[20] such a transformation cannot be applied. Inverting $v=\sigma'(u)$ we obtain[9]

$$u(v)=\begin{cases}-\left(\dfrac{1}{\sigma_\gamma}(\sigma_1-v)\right)^{1/(\gamma-1)} & \text{if } v<-\sigma_1,\\ 0 \quad \text{if } -\sigma_1\leqslant v\leqslant\sigma_1,\\ \left(\dfrac{1}{\sigma_\gamma}(v-\sigma_1)\right)^{1/(\gamma-1)} & \text{if } v>\sigma_1.\end{cases}\tag{10}$$

By inserting Eq. (10) into Eq. (9) we arrive at the free boundary problem:

$$\frac{\partial}{\partial t}v=(\gamma-1)\mu(u)\sigma_\gamma^{1/(\gamma-1)}(v-\sigma_1)^{(\gamma-2)/(\gamma-1)}\frac{\partial^2}{\partial x^2}v \quad \text{for } x\in\left[0,\frac{\zeta L}{4}\right]\tag{11}$$

and

$$\frac{\partial^2}{\partial x^2} v = 0 \quad \text{for } x \in \left[\frac{\zeta L}{4}, \frac{L}{4}\right], \tag{12}$$

where $\zeta \in [0,1]$ is a time-dependent free boundary. Here $\zeta < 1$ means the existence of facets of size $2(1-\zeta)L$ at the tips of the profile. The solution of Eq. (12) taking into account point symmetry is

$$v(x,t) = \sigma_1 \frac{L-4x}{L-\zeta(t)L}. \tag{13}$$

The boundary conditions for Eq. (11) are

$$v'\left(\frac{\zeta L}{4}, t\right) = -\frac{4\sigma_1}{L-\zeta(t)L} \quad \text{and} \quad v'(0,t) = 0. \tag{14}$$

Equation (11) cannot be simply solved by a scaling ansatz as in the case of Eq. (6), since this ansatz does not fulfill the boundary conditions. Furthermore, we do not know the precise form of the mobility $\mu(u)$ near the tips. Thus we have to try an approximative or a numerical solution. In the step flow dominated region of not too small slope, which for our $T=0$ simulations covers the whole profile except the tips where step-step annihilation takes place we can safely use Eq. (5) for the mobility. At the facet edges, however, the solution is determined by the boundary conditions. As a first approximation we use a power series ansatz up to second order in x, namely, $v - \sigma_1 = a_0(t)(1 - 16x^2/\zeta^2 L^2)$, which fulfills the boundary condition with $a_0(t) = \sigma_1 \zeta/(2-2\zeta)$ but solves Eq. (11) up to second order in x only in the singular limit $\zeta \to 1$. For $\zeta \approx 1$ we approximately find $(\partial/\partial t)\,\zeta(t) = -\mu_1(\gamma-1)\sigma_1/L^2 = -c_1$, which leads to

$$\zeta = c_0 - c_1 t, \tag{15}$$

with a constant c_0 determined by the initial condition. For the amplitude of the profile we find

$$h\left(\frac{\zeta L}{4}, t\right) = \frac{L}{4}\left(\frac{\sigma_1}{2\sigma_\gamma}\right)^{1/(\gamma-1)} \frac{(c_0 - c_1 t)^{\gamma/(\gamma-1)}}{(1-c_0+c_1 t)^{1/(\gamma-1)}} \times \int_0^1 (1-y^2)^{1/(\gamma-1)} dy \tag{16}$$

and the profile shape for $\gamma = 3$ is

$$h(x,t) = \frac{2}{\pi} h\left(\frac{\zeta L}{4}, t\right)\left[\frac{4x}{\zeta L}\sqrt{1-\left(\frac{4x}{\zeta L}\right)^2} + \arcsin\left(\frac{4x}{\zeta L}\right)\right]. \tag{17}$$

We note that the solution up to this order is of scaling form and the time dependence enters only via $\zeta(t)$. By adding a term $a_1(t)(1 - 16x^2/\zeta^2 L^2)^2$ we can solve Eq. (11) up to fourth order in x for arbitrary ζ. If we assume $a_1 \ll a_0$ we can solve the emerging differential equation for ζ numerically, which gives the time dependence of the decay and fulfills the assumption $a_1 \ll a_0$ self-consistently. For $\zeta \approx 1$ we recover Eqs. (15)–(17).

B. Simulational results and discussion

Figure 3 displays simulational data of initial sinusoidal grooves on square lattices. The corresponding values of system size L, initial height h_0, number of Monte Carlo steps t, and number of independent runs are given in Table I. The data have been averaged in the transverse direction and over the independent runs. We fitted the profiles with Eq. (17) taking the actual amplitude as $h(4x/\zeta L)$ and used ζ as fit parameter. The values for the absolute deviations Δh_{fit} of the fits and for ζ_{fit} are also displayed in Table I. We cannot decide wether the remaining small but systematical deviations from Eq. (17) are due to higher-order terms of the solution of Eq. (11) or caused by our approximation leading to Eq. (9). As for the step trains, the singularity at the facet edge and also the facet itself are blurred by step fluctuations. Since ζ tends to 1 for larger L we do not expect to find a macroscopic facet for $L \to \infty$. Equation (16), which describes the time dependence of the amplitude, could not be tested seriously with the data of Fig. 3 since the time evolution was too short to pin down the three independent parameters of Eq. (16) precisely. Nevertheless the values of c_0 and c_1 via Eq. (15) give an alternative estimate for the time evolution of ζ that shows a considerably faster decay than the direct evaluation via Eq. (17). This indicates that Eqs. (15)–(17) do not tell the full story and higher-order terms in the solution of Eq. (11) are necessary to describe the full time dependence of the decay.

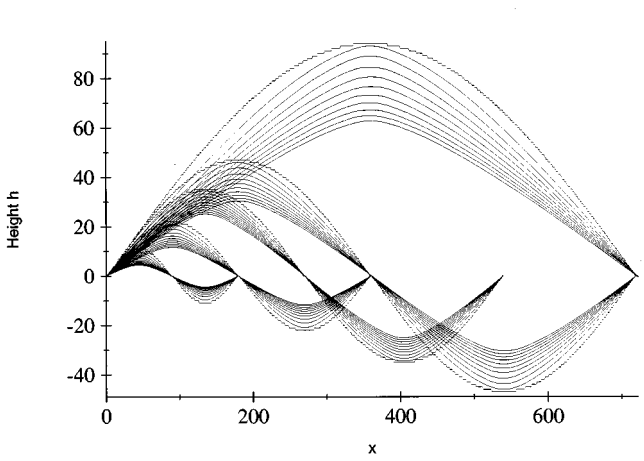

FIG. 3. Flattening sequences of periodic sinusoidal grooves with the same initial slope on quadratic lattices of $L = 180$, 360, 540, 720, and 1440.

To test the wavelength dependence of the decay we in Fig. 4 plot the scaled amplitude $\bar{h} = h/L$ against the scaled time $\bar{t} = t/L^2$. The upper five curves of Fig. 4 display the scaled amplitude for $L = 1440$, 720, 540, 360, and 180 from top to bottom. The lower set of curves shows the same se-

TABLE I. Parameter for the simulational data of Fig. 3.

L	h_0	$10^4 t$	Runs	ζ_{fit}	Δh_{fit}
180	11.85	1.5	10^3	0.89–0.93	0.05
360	23.7	4	200	0.96	0.1
540	35.5	4	100	0.97	0.1
720	47.5	10	20	0.98	0.2
1440	94.5	40	5	0.99	0.4

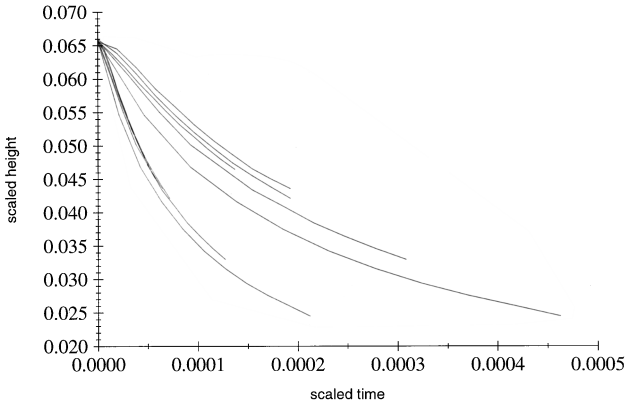

FIG. 4. The upper five curves display the time evolution of the scaled amplitudes h/L for the data of Fig. 3 plotted versus the scaled time t/L^2. The lower set displays the same data plotted versus a differently scaled time $t/L^{2.15}$. In each set from top to bottom data for the system sizes $L=1440$, 720, 540, 360, and 180 are displayed.

quence of data with a different time scaling $t/L^{2.15}$. The obvious violation of the expected scaling cannot be traced back to our approximations, since already Eq. (8) is invariant under reparametrization. We can think of at least two possible sources. We start with a set of straight steps that roughen at the beginning of the decay. This feature is not present in our continuum approach and might introduce an additional L dependence. Secondly the step-step annihilation at the tips of the profile may induce a L dependence of the mobility not present in the case of a step train. Actually, Tang in his recent work did find evidence for logarithmic corrections to the expected scaling due to the top step annihilation process.[23]

To describe the profile form Tang modifies the equation of Lançon and Villain[7] by adding a term proportional to $s_0^2(\partial^2 h/\partial x^2)$, where the function $s_0(t)$ is determined self-consistently out of the width of the topmost terrace. This approach, leading to fits for the profile shape of an accuracy comparable to ours, effectively introduces a mobility $\mu(0) \neq 0$ as we did, but in contrast to our description Tang ignores the wedge singularity of the free energy which led us to the free boundary problem. Thus Tang[23] conjectures that the equation of Lançon and Villain becomes exact in the limit $L\to\infty$. In contrast we expect the solution of the free boundary problem, i.e., Eqs. (15)–(17) plus small corrections due to higher orders, to be valid for $L\to\infty$. The different predictions for the profile shape in the limit $L\to\infty$ are displayed in Fig. 5. One finds that the theory of Lançon and Villain predicts more pronounced tips than the solution of the free boundary problem for both $\gamma=2$ and $\gamma=3$. Our largest simulations of wavelength 1440 support Eq. (17) but they presumably can also be fitted with the term induced by Tang.[23] Further effort is necessary to establish the wavelength dependence for periodic grooves.

V. CONCLUSION

In conclusion, we showed that our large-scale $T=0$ simulations of step trains agree quantitatively with the predictions of continuum theory below the roughening transition. For periodic grooves we used a nonzero mobility $\mu(0)$ in the continuum theory to capture some of the subtleties of step-step annihilation. Our approximate solution for the profile shape is in good agreement with the simulations while for time decay and wavelength scaling discrepancies remain.

One can extend our simulation to temperatures $T>0$ to study the influence of nucleation on surface free energy and mobility. One can also incorporate surface diffusion dynam-

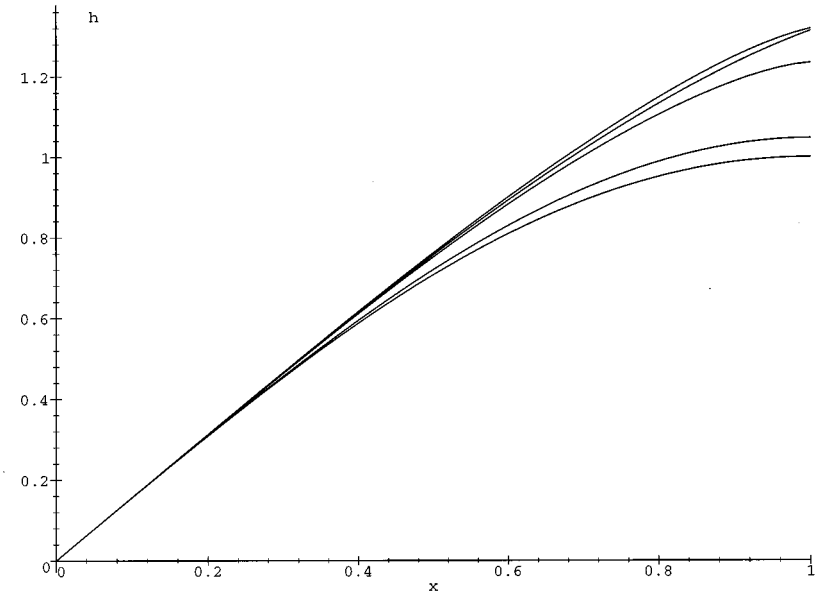

FIG. 5. Different predictions for the profile shape in the limit $L\to\infty$ are plotted with the same initial slope at $x=0$. From top to bottom the curves are numerical solution of Eq. (4) [after a separation ansatz $h(x,t)=g(t)f(x)$] with $\gamma=3$ (topmost) and $\gamma=2$, approximate solutions of the free boundary problem (with $\zeta=1$) for $\gamma=3$ [Eq. (15)] and $\gamma=2$, and a sine-function for comparison.

ics in our kind of algorithm. This would be interesting since the existing simulations[3,21,22] use systems too small for a comparison to continuum theory.

ACKNOWLEDGMENTS

I thank L. Schäfer, H. Spohn, and M. Rost for carefully reading the manuscript, S. Müller for further tips for the presentation, and J. Krug for providing me with a copy of Ref. 23. This work was supported by the Deutsche Forschungsgemeinschaft SFB 237 Unordnung und gross e Fluktuationen.

APPENDIX

Here we give the logical function that counts the number of atoms on the six in-plane next-nearest-neighbor sites for a given evaporation or condensation site. This function is the main extension of the code given already in Ref. 11. Let $is(i)\in\{0,1\}$ denote the value of the spin on an evaporation or condensation site and $is(j)$ with $j\in\{1,...,6\}$ in some arbitrary order, the values of the spins on the six next-nearest-neighbor sites of site i. We define the flag $f_j:=is(j)\uplus is(i)$, which has the values

$$f_j=\begin{cases}0 & \text{if } h(j)=h(i) \quad (\text{occupied site } j)\\ 1 & \text{if } h(j)=h(i)-3 \quad (\text{empty site } j)\end{cases} \tag{A1}$$

for i being an (occupied) evaporation site, and

$$f_j=\begin{cases}0 & \text{if } h(j)=h(i) \quad (\text{empty site } j)\\ 1 & \text{if } h(j)=h(i)+3 \quad (\text{occupied site } j)\end{cases} \tag{A2}$$

for i being a (empty) condensation site. Thus f_j is the occupation number of site j if site i is a condensation site f_j if i is an evaporation site. Out of the f_j we now create flags n_k with the value 1 for k occupied next-nearest-neighbor sites, being 0 otherwise:

$$n_0=\neg(f_1\cup f_2\cup f_3\cup f_4\cup f_5\cup f_6), \tag{A3}$$

$$n_1=(f_1\uplus f_2\uplus f_3\uplus f_4\uplus f_5\uplus f_6)\cap\neg\{[(f_1\cap f_2)\cup(f_3\cap f_4)\cup(f_5\cap f_6)]\cup[(f_1\cap f_2)\cup(f_3\cap f_5)\cup(f_4\cap f_6)]\cup[(f_1\cap f_2)\cup(f_3\cap f_6)\cup(f_4\cap f_5)]\}, \tag{A4}$$

$$n_2=(f_1\cup f_2\cup f_3\cup f_4\cup f_5\cup f_6)\cap[\neg(f_1\uplus f_2\uplus f_3\uplus f_4\uplus f_5\uplus f_6)]\cap[\neg\{[(f_1\cap f_2)\cup(f_3\cap f_4)\cup(f_5\cap f_6)]\cap[(f_1\cap f_3)\cup(f_2\cap f_5)\cup(f_4\cap f_6)]\}], \tag{A5}$$

$$n_4=[\neg(f_1\cap f_2\cap f_3\cap f_4\cap f_5\cap f_6)]\cap[\neg(f_1\uplus f_2\uplus f_3\uplus f_4\uplus f_5\uplus f_6)]\cap\{[(f_1\cup f_2)\cap(f_3\cup f_4)\cap(f_5\cup f_6)]\cup[(f_1\cup f_3)\cap(f_2\cup f_5)\cap(f_4\cup f_6)]\}, \tag{A6}$$

$$n_5=(f_1\uplus f_2\uplus f_3\uplus f_4\uplus f_5\uplus f_6)\cap\{[(f_1\cup f_2)\cap(f_3\cup f_4)\cap(f_5\cup f_6)]\cap[(f_1\cup f_2)\cap(f_3\cup f_5)\cap(f_4\cup f_6)]\cap[(f_1\cup f_2)\cap(f_3\cup f_6)\cap(f_4\cup f_5)]\}, \tag{A7}$$

$$n_6=(f_1\cap f_2\cap f_3\cap f_4\cap f_5\cap f_6). \tag{A8}$$

Note that we listed the flags n_k for the case of i being a condensation site, and one has to replace all f_j by $\neg=f_j$ in the case of i being a evaporation site. With these flags at hand we can construct expressions for the missing n_3 and for $n_{\{3,\ldots,6\}}=\neg(n_0\cup n_1\cup n_2)$ and $n_{\{0,\ldots,3\}}=\neg n_6\cup n_5\cup n_4)$, which we need to apply the Metropolis rates (1) and (2).

[1] W. W. Mullins, J. Appl. Phys. **28**, 33 (1957); **30**, 7 (1959).

[2] K. Yamashita, H. P. Bonzel, and H. Ibach, Appl. Opt. **25**, 231 (1981).

[3] Z. Jiang and C. Ebner, Phys. Rev. B **40**, 316 (1989); **53**, 11 146 (1996).

[4] W. Selke and T. Bieker, Surf. Sci. **281**, 163 (1993).

[5] W. Selke and P. M. Duxbury, Z. Phys. B **94**, 311 (1994).

[6] A. Rettori and J. Villain, J. Phys. I **49**, 257 (1988).

[7] F. Lançon and J. Villain, Phys. Rev. Lett. **64**, 293 (1990); in *Kinetics of Ordering and Growth at Surfaces*, Vol. 239 of *NATO Advanced Study Institute Series B: Physics*, edited by M. G. Lagally (Plenum, New York, 1990), p. 369.

[8] H. Spohn, J. Phys. I **3**, 69 (1993).

[9] J. Hager and H. Spohn, Surf. Sci. **324**, 365 (1995).

[10] H. P. Bonzel and E. Preuss, Surf. Sci. **336**, 209 (1995) and references therein.

[11] B.-M. Forrest and L. H. Tang, J. Stat. Phys. **60**, 181 (1990).

[12] H. W. J. Blöte and H. J. Hilhorst, J. Phys. A **15**, L631 (1982).

[13] L. H. Tang, B. M. Forrest, and D. E. Wolf, Phys. Rev. A **45**, 7162 (1992).

[14] M. M. Gruber and W. W. Mullins, J. Phys. Chem. Solids **28**, 875 (1966).

[15] D. G. Aronson, in *Nonlinear Diffusion Problems*, edited by A. Fasano and M. Primicerio, Lecture Notes in Mathematics Vol. 1224 (Springer, Berlin, 1986), p. 1.

[16] G. I. Barenblatt, *Scaling, Self-similarity, and Intermediate Asymptotics*, Cambridge Texts in Applied Mathematics 14 (Cambridge University Press, Cambridge, 1996), p. 167.

[17] W. Selke, in *Proceedings of the 8th Joint APS-EPS International Conference on Physics Computing*, edited by P. Borcherds, M. Bubak, and A. Maksymowicz (Academic Computer Centre CYFRONET, Krakow), p. 443.

[18] W. Selke and P. M. Duxbury, Phys. Rev. B **52**, 17 468 (1995).

[19] L. H. Tang (unpublished).

[20] C. Duport, A. Chame, W. W. Mullins, and J. Villain, J. Phys. (France) **6**, 1095 (1996).

[21] P. C. Searson, R. Li, and K. Sieradzki, Phys. Rev. Lett. **74**, 1395 (1995).

[22] M. V. Ramana Murty and B. H. Cooper, Phys. Rev. B **54**, 10 377 (1996).

[23] L. H. Tang, in *Dynamics of Crystal Surfaces and Interfaces*, edited by P. M. Duxbury and T. Pence (Plenum, New York, 1997), p. 169.